

# **An Efficient Continuous Hydrothermal Flow Synthesis of Carbon Quantum Dots from a Targeted Biomass Precursor for On-Off Metal Ions Nano-Sensing**

Ioan-Alexandru Baragau,<sup>a</sup> Nicholas P. Power,<sup>b</sup> David J. Morgan,<sup>c</sup> Richard A. Lobo,<sup>d</sup> Christopher S. Roberts,<sup>e</sup> Maria-Magdalena Titirici,<sup>d</sup> Vesna Middelkoop,<sup>f</sup> Adriana Diaz,<sup>g</sup> Steven Dunn<sup>a</sup> and Suela Kellici<sup>a\*</sup>

<sup>a</sup> School of Engineering, London South Bank University, 103 Borough Road, London, SE1 0AA, UK

\*E-mail: [kellcis@lsbu.ac.uk](mailto:kellcis@lsbu.ac.uk), Website: [www.nano2d.co.uk](http://www.nano2d.co.uk)

<sup>b</sup> School of Life Health & Chemical Sciences, Open University, Walton Hall, Milton Keynes, MK7 6AA, UK

<sup>c</sup> Cardiff Catalysis Institute, School of Chemistry, Cardiff University, Park Place, Cardiff, CF10 3AT, UK

<sup>d</sup> Department of Chemical Engineering, Imperial College, South Kensington, London, SW7 2AZ, UK

<sup>e</sup> Department of Chemistry, Imperial College, South Kensington, London, SW7 2AZ, UK

<sup>f</sup> Vlaamse Instelling voor Technologisch Onderzoek – VITO, Boeretang 200, 2400 Mol, Belgium

<sup>g</sup> Ecodesign, Schwindgasse 4/2 1040 Vienna, Austria

**Abstract:** Glucose, a readily available biomass precursor is used for the production of carbon quantum dots (CQDs) via a fast, efficient, and environmentally benign continuous hydrothermal flow synthesis (CHFS) process using supercritical water, an approach that can readily be scaled-up for industrialization, producing materials with enhanced properties. The water soluble CQDs exhibit an average particle size of  $2.3 \pm 0.5$  nm, with optimum emission intensity at 446 nm on excitation at 360 nm. The as-synthesized CQDs with no extra modification show promising sensitivity and good selectivity for the highly toxic, carcinogenic, and mutagenic chromium (VI) ion (limit of detection of 1.83 ppm) and for the essential bioactive transition metal, iron (II) ion (limit of detection of 6.09 ppm). The life-cycle assessment confirms that in comparison to conventional batch synthetic method, continuous hydrothermal flow synthesis process is significantly a more efficient and greener route for the synthesis of carbon quantum dots from the glucose biomass precursor.

**Keywords:** biomass, carbon quantum dots, continuous hydrothermal flow synthesis, nano-sensor.

## INTRODUCTION

Maximising the conversion of biomass and waste-related components into valuable products or nanomaterials is one of the most significant challenges for a sustainable future. In recent years there has been a fast-paced exponential development and diversity of biomass derived materials, and in particular, the next generation carbon-based nanomaterials (nanotubes, 2D nanosheets of graphene, fullerenes, etc.) that have found multiple applications in optoelectronics, photocatalysis, light-emitting devices, solar cells, bio-related (e.g bio-markers and drug delivery), anticounterfeit (e.g. fluorescent inks), and ion sensors.<sup>1,2</sup> Particularly, luminescent nanomaterials such as carbon quantum dots (CQDs) have attracted much scientific interest since their 2004 discovery by *Xu et al.*<sup>3</sup> Typically, CQDs are nanometric-range particles (< 10 nm in diameter), able to absorb and emit light at certain wavelengths, due to their graphitic core and/or amorphous carbon framework (sp<sup>2</sup>/sp<sup>3</sup> carbon) surface, richly coated with oxygen functionalities and/or defects<sup>4</sup>. CQDs materials, which exhibit features such as outstanding optical properties and photostability, biocompatibility, and low capacity for hazardous environmental impact, are indeed highly desirable in a variety of applications.

Producing CQDs from biomass-related compounds such as glucose,<sup>5,6</sup> fructose,<sup>7</sup> citric acid,<sup>8</sup> chitosan,<sup>9</sup> cellulose<sup>10</sup> or lignin,<sup>11</sup> through intra- and inter-molecular dehydration and/or decomposition processes under hydrothermal conditions is one of the more efficient bottom-up approaches.<sup>8,12</sup> Whilst a wide range of raw biomass sourced materials (coffee grounds, leaves, guano)<sup>13–15</sup> can be used via this approach for synthesis, materials of known elemental provenance allow for a more useful control in their design and synthesis. An alternative approach to the bottom-up method is the cutting of higher dimensional pre-synthesised carbon materials such as 1D carbon nanotubes<sup>16</sup>, 3D graphite<sup>17</sup>, or carbon black<sup>18</sup>, to reduced 0D dimensions dots, lower than 10 nm particle size; the top-down approach to producing CQDs.

The production of CQDs *via* hydrothermal bottom-up methods involves the carbon precursors reaction mixture being exposed from a few hours right up to 48 hours at temperatures between 150-250 °C in batch hydrothermal processes,<sup>4,19</sup> all of which involve both significant energy consumption and time. Therefore, an approach for the synthesis of carbon dots from biomass related precursor that minimizes the process duration and energy consumption is needed. As such, Continuous Hydrothermal Flow Synthesis (CHFS), a bottom-up hydrothermal approach, offers an affordable way to produce customized and an advanced development in biomass related carbon materials with real-time full command of the reaction parameters. It is a

one-step process that involves the mixing of supercritical water flow with one or more water-soluble precursor flows in a counter flow mixing point reactor, with reactions occurring within seconds. CHFS approaches have been successfully applied within this laboratory in materials synthesis such as metal oxides,<sup>20</sup> nanometals,<sup>21</sup> 2D materials,<sup>22–25</sup> nanocomposites<sup>26</sup> and nitrogen-doped CQDs.<sup>27</sup> This method is proven in reducing the complexity of traditional batch processes and can be readily scaled up for the production of nanomaterials such as CQDs, giving high quality and reproducibility for a homogenous product with optimised properties.

An interesting aspect for some CQDs is the predilection of their entangled functionalized surface to interact through an impressive degree of selectivity and sensitivity to ions or molecular compounds in solution allowing an optical response (fluorescence enhancement or quenching). Examples from the literature demonstrating fluorescent response harnessed as nano-sensors include those for ions such as Fe(III),<sup>28,29</sup> Cr(VI),<sup>20</sup> Cu(II),<sup>30</sup> Hg(II),<sup>31</sup> molecular compounds,<sup>32–34</sup> and pH.<sup>35</sup> The sensing and selective detection of different analytes such as metal ions, anions, organic molecules, metal nanoparticles and biological samples can be engineered and designed into CQDs. This nano-sensing process can be controlled by the inclusion/alteration of the surface-functional groups for which the optical properties of CQDs are affected when in contact with the analyte.

In this work, CQDs were synthesized via a green, fast and energy efficient single step continuous hydrothermal flow synthesis approach using a low-cost readily available biomass carbon source, glucose; extensively used in batch hydrothermal synthesis methods as a model platform for waste and biomass utilization and recovery.<sup>36,37</sup> The CQDs obtained exhibited green-blue fluorescence, and owing to their fluorescence stability under neutral mild acidic and basic conditions, the CQDs were successfully tested as a fluorescent nano-sensor for the sensing of Cr (VI) and Fe (II) ions with favourable sensitivity and selectivity over other ions and anions. Their dual-ion affinity<sup>38</sup> offers the opportunity to apply the CQDs nanosensor for iron (II) detection in biomedical quantification in blood samples or living cells,<sup>39,40</sup> or for chromium (VI) detection and quantification in soil or surface/industrial water effluent.<sup>41</sup>

## EXPERIMENTAL SECTION

**Chemicals:** All materials were purchased from UK based commercial suppliers: Sigma-Aldrich, except C<sub>6</sub>H<sub>12</sub>O<sub>6</sub>, K<sub>2</sub>CrO<sub>4</sub>, and K<sub>2</sub>Cr<sub>2</sub>O<sub>7</sub> which were purchased from Fisher Scientific. All

chemicals were used as received. Deionized water (15 M $\Omega$ , ELGA Purelab system) was used in all experiments. The aqueous solutions of metal ions used for the nano-sensing experiment were made from either their nitrate (Ag<sup>+</sup>, Co<sup>2+</sup>, Ni<sup>2+</sup>, Fe<sup>3+</sup>, Cr<sup>3+</sup>, Ce<sup>3+</sup>), acetate (Fe<sup>2+</sup>, Zn<sup>2+</sup>, Cu<sup>2+</sup>), or chloride (Na<sup>+</sup>, K<sup>+</sup>, Mg<sup>2+</sup> and Ca<sup>2+</sup>) and sodium (F<sup>-</sup>, Cl<sup>-</sup>, Br<sup>-</sup>, I<sup>-</sup>, NO<sub>3</sub><sup>-</sup>, H<sub>2</sub>PO<sub>4</sub><sup>-</sup>, CH<sub>3</sub>COO<sup>-</sup>, HCOO<sup>-</sup>, HCO<sub>3</sub><sup>-</sup>, SO<sub>4</sub><sup>2-</sup> and CO<sub>3</sub><sup>2-</sup>).

## Characterisation

CQDs were analysed using high-resolution transmission electron microscopy (HRTEM) (JEOL JEM2100 operated at 200 kV and 107 $\mu$ A; data analysis performed *via* ImageJ software), atomic force microscopy (AFM) (hpAFM tapping mode; data analysis performed using NMI Image Analyser (v1.4, NanoMagnetics Instruments), X-Ray photoelectron spectroscopy (XPS) (Thermo Fisher Scientific K-alpha+ spectrometer; data analysis was done using in CasaXPS software), Raman spectroscopy (Bruker, SENTERRA II,  $\lambda_{ex}$  = 532 nm), fourier-transform infrared spectroscopy (FT-IR) (Shimadzu IRAffinity-1S). Optical properties were studied using spectrophotometry for absorption studies (UV-Vis spectrophotometer, Shimadzu UV-1800) and photoluminescence (PL) (Shimadzu RF-6000). Specific characterisation methodologies including the quantum yield value determination (see Figure S1) were performed as described previously.<sup>27</sup>

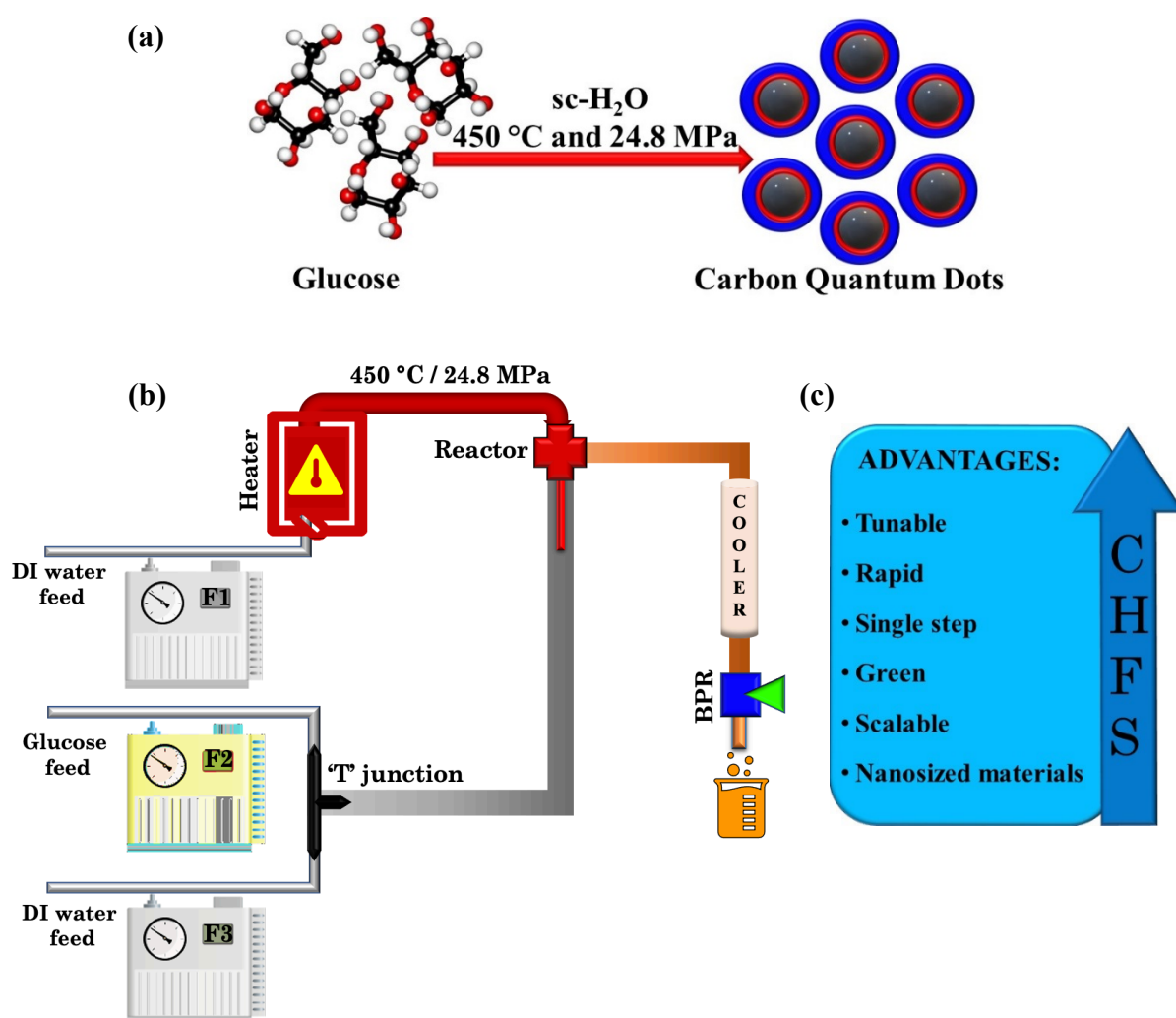
## Chromium (VI) and Fe (II) ion-sensing:

To determine the PL sensing properties (sensitivity and selectivity) of CQDs towards Cr (VI) and Fe (II), the following experiments were conducted: Cr (VI) and Fe (II) stock solutions (1000 ppm) were prepared by dissolving potassium chromate (K<sub>2</sub>CrO<sub>4</sub>, 100 mg) or iron acetate (Fe(C<sub>2</sub>H<sub>3</sub>O<sub>2</sub>)<sub>2</sub>, 100 mg) in deionized water (100 mL) using standard volumetric flasks. To a fresh stock of CQD solution (1.23 mg/mL) in a standard volumetric flask (10 mL), was added the necessary volume of 1000 ppm Cr (VI) or Fe (II) stock solutions to achieve the following concentrations of interest which were: 500 ppm, 250 ppm, 100 ppm, 75 ppm, 50 ppm, 20 ppm, 10 ppm, 5 ppm and 1 ppm. The spectral PL response of each corresponding solution was recorded after 3 minutes incubation. Each ion-sensing experiment for the quantitative analysis of Cr (VI) or Fe (II) was repeated three times. The PL experimental set conditions were as follows:  $\lambda_{ex}$  = 360 nm, 5 nm band-slits (excitation and emission), sensitivity = fixed at high, response time = 0.5 s, emission spectrum range: 370 - 650 nm, PL intensity at  $\lambda_{em}$  = 446 nm was used for all quantitative analysis experiments. A range of anions and various metal cations at 50 ppm as a standard concentration were tested to demonstrate selectivity and sensitivity.

Furthermore, the CQDs stability in presence of Cr (VI) or Fe (II) (50 ppm) was demonstrated by monitoring the fluorescence intensity of each corresponding solution in a continuous mode for 1200 seconds at  $\lambda_{ex} = 360$  nm (see Figure S2).

### Synthetic Methodology:

The procedure for Continuous Hydrothermal Flow Synthesis (CHFS) of CQDs procedure for CQDs via CHFS is illustrated in Schematic 1.



**Schematic 1:** Production of carbon quantum dots (CQDs) *via* Continuous Hydrothermal Flow Synthesis (CHFS) approach: (a) graphical representation of the synthetic route employing glucose as carbon precursor and supercritical water (sc-H<sub>2</sub>O) as solvent and reaction environment, (b) simplified CHFS reactor design (Key: F = feeds of water and glucose precursor delivered to the reactor by high pressure pumps, BPR = back-pressure regulator), and (c) CHFS advantages.

The CHFS system employs the following feeds: supercritical water (sc-H<sub>2</sub>O) feed (F1: flow rate: 20 mL min<sup>-1</sup>) and the glucose carbon precursor feed (F2: with concentration of 70 mg mL<sup>-1</sup>, flow rate: 5 mL min<sup>-1</sup>) and a second deionized water feed (F3: flow rate 5 mL min<sup>-1</sup>). The ‘blank’ feed of deionised water maintains the optimal reaction conditions of the system for CQDs synthesis *via* CHFS in terms of the global flow rate, pressure, temperature, and carbon precursor in the reaction area.<sup>27</sup> The sc-H<sub>2</sub>O feed (F1) was supplied at 450 °C and system pressure at a constant 24.8 MPa *via* a back-pressure regulator (“BPR”). Feeds F2 and F3 were merged *via* a “T” junction prior to contact with the supercritical water feed (F1) at the reaction zone (“Reactor”) where CQDs were generated. The reactor effluent containing the CQDs was then cooled in a straight pipe-in-pipe water cooler (labelled as “Cooler”), passing *via* “BPR” for collection and further processing (see Schematic 1). The reaction time in the “Reactor” occurs in fraction of second and the overall time from injection of the precursors to collection point is *ca.* 2 mins. The reactor was run for 40 mins. Filtration of the CHFS synthesised CQDs reaction product was initially through a 0.2 µm alumina membrane, followed successively by a 30 kD and then 1kD membranes in a tangential filtration unit, with the final solution concentrated to 1/5 of its initial volume. A small volume of purified carbon dot (10 mL) was freeze dried (Heto PowderDry PL 3000) providing a sample concentration of 1.23 mg mL<sup>-1</sup>.

## RESULTS AND DISCUSSION

Carbon quantum dots are very attractive material due to their optical and chemical properties, especially their emissions in the visible range.<sup>4,6</sup> The CHFS approach allows for the continuous mode of production of CQDs by simply using glucose as the carbon source, *via* supercritical hydrothermal conditions (P = 24.8 MPa and T = 450 °C). The structural/compositional, morphological and optical properties of the as-produced CQDs were characterized using a variety of techniques and discussed as follows.

HRTEM images (Figure 1 a-d) of the as-prepared CQDs display an irregular round shape exhibiting a mean particle size of  $2.3 \pm 0.5$  nm (particle size distribution range between 1.4 nm to 4.5 nm), Figure 1d. This was consistent, within experimental error, with the observed tomography derived from atomic force microscopy (AFM) (Figure 1e-d) exhibiting an average value of  $3.5 \pm 1.7$  nm (with distribution range from 1.0 to 9 nm) for the CQDs. Both systems of analysis reflect excellent homogeneity for the CQDs produced by CHFS. The in-plane lattice

spacing of 0.22 nm (Figure 1c) is as expected for a graphitic core arrangement is as expected for a graphitic core arrangement of the carbon atoms and is in-line with previously reported literature.<sup>42,43</sup>

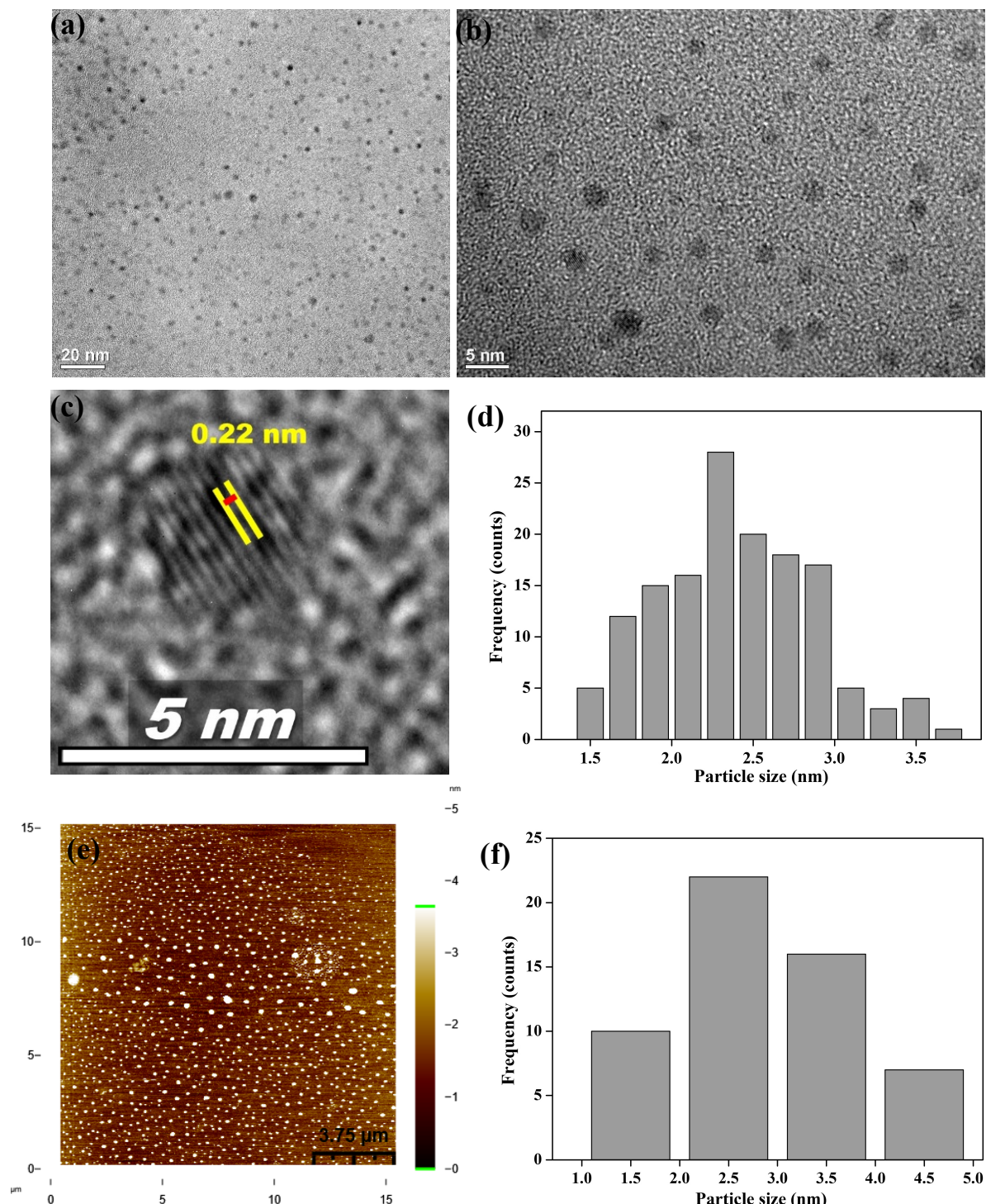


**Figure 1:** HRTEM images of glucose derived carbon quantum dots obtained at (a) 20 nm, (b) 5 nm imaging scale with (c) showing graphitic core lattice fringes, (d) particle size distribution histogram (mean particle size of  $2.3 \pm 0.5$  nm). (e) AFM tomographic image and (f) particle size distribution histogram.

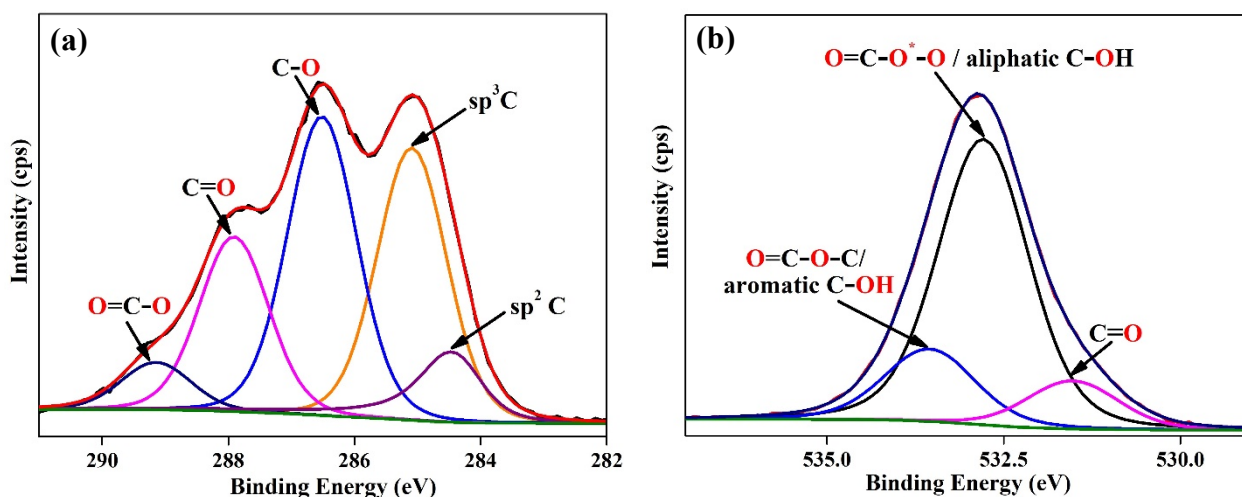


**Figure 2:** XPS spectra of (a) C(1s) and (b) O(1s) regions showing the composition and surface chemistry of CQDs.

X-ray photoelectron spectroscopy (XPS) analysis<sup>44</sup> of the surface chemistry of the CQDs provided a C(1s) spectra (Figure 2a) exhibiting peaks at 284.4 (sp<sup>2</sup>, C-C), 285 (sp<sup>3</sup>, C-C), 286.5 (C-O), 287.9 (C=O) and 289.2 eV (-O-CO-), whereas the O(1s) spectra (Figure 2a) exhibited asymmetry to both lower and higher binding energy sides of the peak maxima which was best fitted to three species with binding energies of 531.5 (C=O), 532.7 (O-CO\*-O / aliphatic C-OH) and 533.5 eV (O-CO-C / O-C-O / aromatic C-OH). This diversity of oxygen functionalities of the CQDs surface is consistent with FT-IR spectroscopy analysis (Figure 3b). Stretches for C=O (COOH) are evident at 1712 cm<sup>-1</sup> and 1658 cm<sup>-1</sup>, those for C-O and C-O-C vibrations assigned at given at 1357 cm<sup>-1</sup> and 1033 cm<sup>-1</sup> respectively,<sup>45</sup> and the broad absorption band at 3302 cm<sup>-1</sup> can be assigned to overlapping stretches for O-H (R-OH, -COOH). Furthermore, the stretches at 2900 cm<sup>-1</sup>, and 1500 cm<sup>-1</sup> and ~ 1600 cm<sup>-1</sup>, assigned to alkyl (sp<sup>3</sup> C-H) and aromatic (sp<sup>2</sup> C-H) vibrations respectively.

Analysis of Raman data gathered for the CHFS synthesised CQDs (Figure 3a) reveal two broad peaks at 1384 and 1597 cm<sup>-1</sup> corresponding to D and G vibrational bands indicating the presence of sp<sup>3</sup>-carbon and the graphitic core (sp<sup>2</sup>-hybridized carbon), respectively. The G-band is recognized as an E<sub>2g</sub> vibrational mode of the graphitic core correlated with the vibration of sp<sup>2</sup> hybridized carbon atoms, suggesting the aromatic character of CQDs. This is consistent with the HRTEM lattice spacing described earlier (Figure 1c) and furthermore, the I<sub>D</sub>/I<sub>G</sub> ratio of 0.83 indicates the predominance of the graphical core in the CQDs. This I<sub>D</sub>/I<sub>G</sub> value lies somewhere between the values of thin graphite flakes and graphite oxide.<sup>46,47</sup> The smaller D-band peak

indicates the disorder in the structure which can be associated with oxygen functionalities. These results are consistent and in agreement with both FTIR and XPS data, the latter indicating a C/O ratio of 1.7 (with O1s: 36.74 at%).

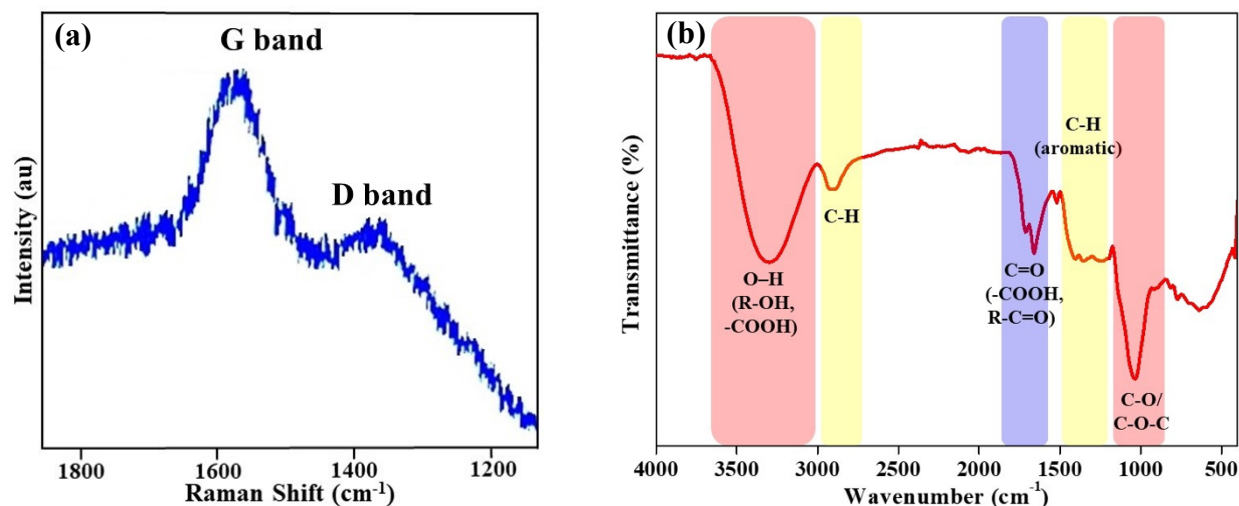


**Figure 3:** (a) Raman and (b) FTIR spectra of CQDs.

The characteristic optical properties corresponding to specific absorption and emission properties of the CQDs in aqueous solutions at varying pH values (Figure 4 (a - d)) were studied using UV-Vis and steady-state photoluminescence spectrophotometry (PL). The UV-Vis spectrum presented two absorption bands, 225 nm which can be assigned as aromatic  $sp^2$   $\pi$ - $\pi^*$  transitions within the graphitic core (C=C and C-C bonds), and 280 nm which can be related to the  $n$ - $\pi^*$  transitions for C=O moieties that are abundantly located in the CQDs surface; both of which are characteristic of CQDs (Figure 4 (a)).<sup>7</sup>

Photoluminescence analysis for the as-synthesised CQDs under UV-Vis excitation (300 – 500 nm) displayed optimal  $\lambda_{ex}$  at 360 nm exhibiting a blue fluorescence emission at  $\lambda_{em} = 446$  nm. This coincided with a blue-shift of the maximum of emission and an increase in the PL intensity from 320 nm to 360 nm excitation wavelengths, and a consecutive subsequent red-shift and a consistent decrease in PL intensity for lower energy excitations (360 - 500 nm), Figure 4b, a typical observed feature of UV-Vis excitation dependent emission behaviour for CQDs.<sup>7,43</sup> The red-shift character observed may be ascribed to a greater predominance of  $\pi$ - $\pi^*$  graphitic core transitions of the isolated  $sp^2$  clusters at lower excitation energies.<sup>48</sup> A quantum yield value of 0.3% (calibrated using as a standard quinine sulphate in 0.1 M H<sub>2</sub>SO<sub>4</sub>) for the as-synthesised

CQDs was determined, which was greater than the negligible QY of carbon dots generated purely from citric acid, but much lower than that recorded for N-doped citric acid CQDS (15%) produced under CHFS conditions previously in our lab (see Figure S3),<sup>27</sup> but still comparable to most reports for CQDs composed of carbon and oxygen without any surface passivation processes.<sup>43,49</sup>

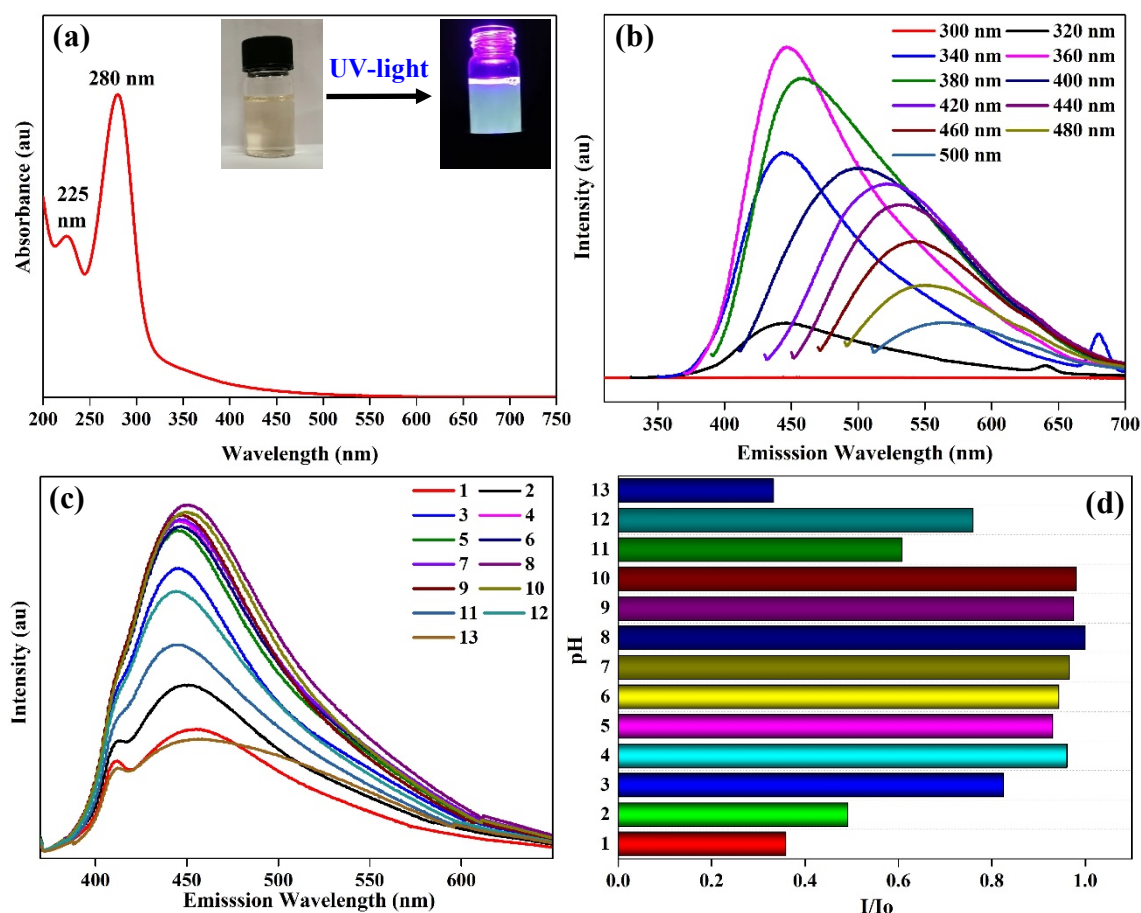


**Figure 4:** (a) UV-Vis absorption spectrum of carbon quantum dots with inset showing CQDs solution under UV-light (365 nm). (b) Photoluminescence spectrum of CQDs at excitation wavelengths between 300 – 500 nm showing excitation dependence performance. pH effect over (c) the emission intensity and (d) data represented in histogram format.

The stability of the CQDs and that of their fluorescence when subjected to the influence of pH change was also investigated since pH can impact on the sensitivity and selectivity of a sensor for metal ions in environmental or biological systems (Figure 4c and 4d). The fluorescence intensity of these CQDs displayed negligible change over a broad pH range (pH 3 to 10), however, in both stronger acidic (pH 1 to 3) and basic (pH 11 – 14) media, the emissive intensity was substantially changed. This diminished intensity can be considered a consequence of greater disruption of the oxygen moieties randomly distributed on the CQDs surface and their

respective fluorescent ability. A small but significant red shift was also observed for the CQD emissions in both the strong acidic and basic solutions. This phenomenon can relate to the missing emissivity from the CQDs surface, thus permitting more prominent emissions from the graphitic core over that of the surface emissions.

### Chromium (VI) and Fe (II) ion-sensing:

Cognisant of both its inherent fluorescent properties and pH stability ranging from pH 3-10, evaluating the CQDs sensitivity towards other ions was considered pertinent.

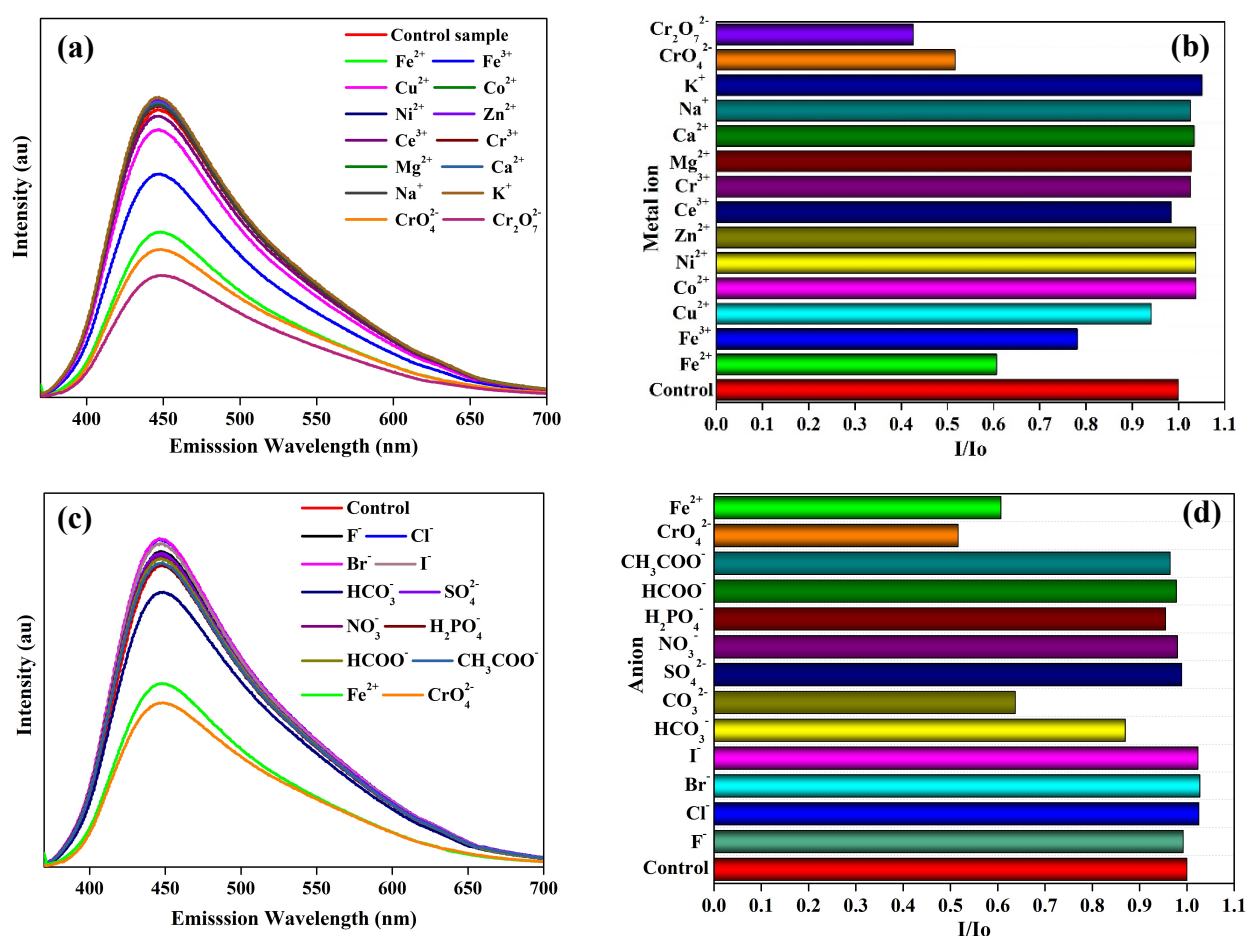


**Figure 5:** Selectivity of the CQDs based chemo-sensor over other (a-b) ions and (c-d) anions.

Further studies determined that the as-synthesized CQDs had a sensitivity for both chromium (VI) (CrO<sub>4</sub><sup>2-</sup>/Cr<sub>2</sub>O<sub>7</sub><sup>2-</sup>), a highly toxic, carcinogenic and mutagenic heavy metal anthropogenic pollutant in water-, and water-soluble iron species,<sup>50-52</sup> Fe (II) and to a lesser extent Fe (III) (Fe<sup>2+</sup> aqueous solubility at pH 7.4 is in the order of 10<sup>-1</sup> versus 10<sup>-18</sup> M for Fe<sup>3+</sup>),<sup>53</sup> an essential bioactive transition metal ion (Fe<sup>2+</sup>/Fe<sup>3+</sup>) whose deficiency (hypoferremia) or excess (hyperferremia) can be detrimental. The CQDs exhibited significant selectivity over a range of

other environmentally relevant cations and anions, including metal ions such as  $\text{Na}^+$ ,  $\text{K}^+$ ,  $\text{Ca}^{2+}$ ,  $\text{Mg}^{2+}$ ,  $\text{Co}^{2+}$ ,  $\text{Ni}^{2+}$ ,  $\text{Cu}^{2+}$ ,  $\text{Zn}^{2+}$ ,  $\text{Cr}^{3+}$ ,  $\text{Ce}^{3+}$ ,  $\text{Ag}^+$ , and the anions:  $\text{F}^-$ ,  $\text{Cl}^-$ ,  $\text{Br}^-$ ,  $\text{I}^-$ ,  $\text{NO}_3^-$ ,  $\text{SO}_4^{2-}$ ,  $\text{HCOO}^-$ ,  $\text{CH}_3\text{COO}^-$ ,  $\text{HCO}_3^-$ ,  $\text{CO}_3^{2-}$ , each in aqueous solutions at concentrations of 50 ppm (Figure 5). (Figure 5). Experiments were performed in triplicate for each ion in all experiments and particularly focussed on chromium (VI) ( $\text{CrO}_4^{2-}/\text{Cr}_2\text{O}_7^{2-}$ ) and Fe (II).

This sensitivity of the CQDs fluorescent probe for Cr (VI) and Fe (II) was investigated further to determine their limits of detection (LOD) and limits of quantification (LOQ).

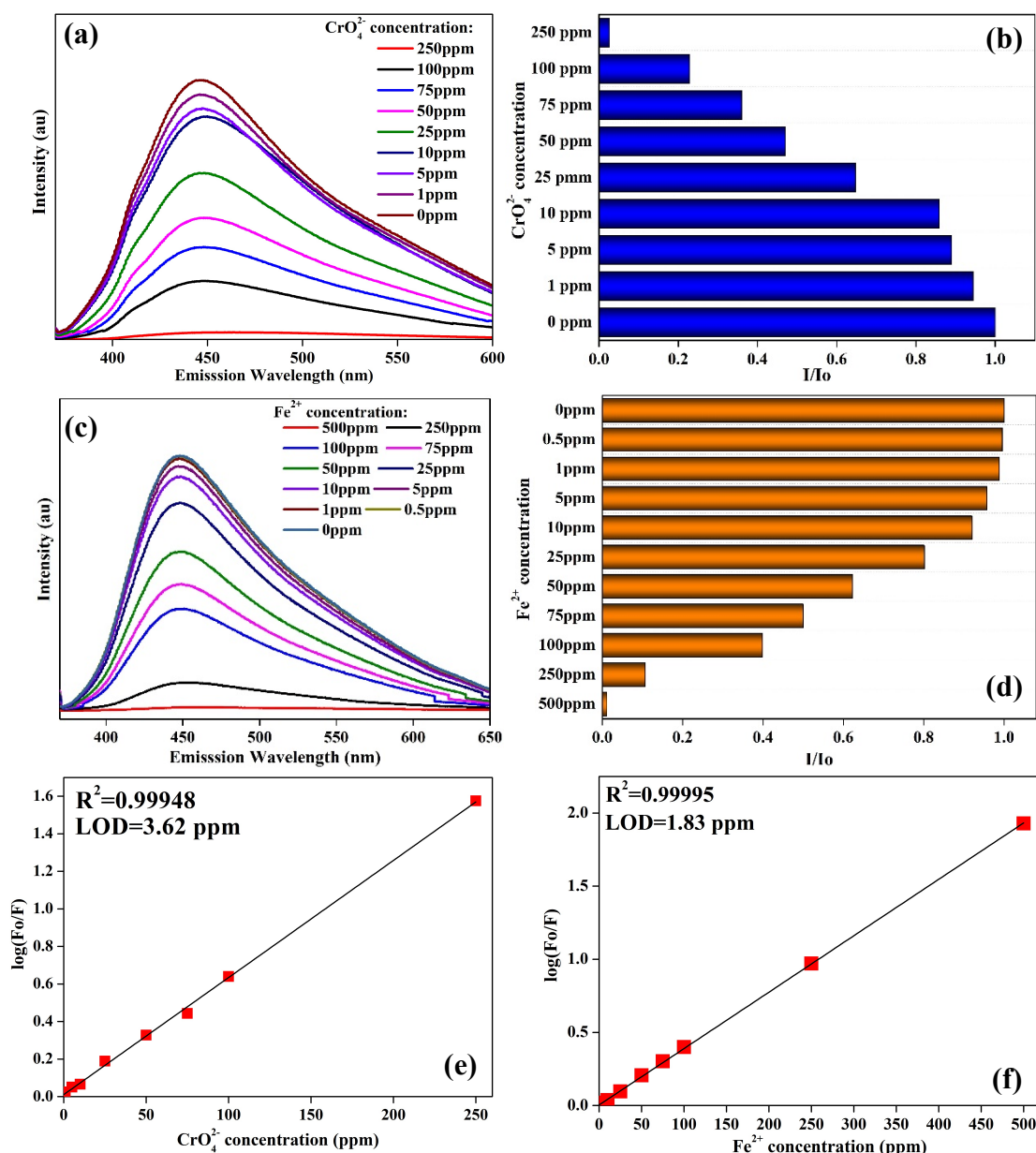


**Figure 6:** Sensitivity of the CQDs based sensor over Cr (VI) and Fe (II) ions. The influence on PL spectrum of CQDs on the fluorescence intensity changes in (a-b) Cr (VI) and (c-d) Fe (II) concentration range (ppm) with (e-f) showing Stem-Volmer graphs as a function of  $\log(F_0/F)$  versus [Cr (VI)] and [Fe (II)] ions.

The fluorescence of CQDs at 446 nm was quenched on the addition of Cr (VI) (Figure 6 a-b) or Fe (II) (Figure 6c-d); the emission intensity decreasing showing linear dependence for the respective increase in concentrations of Cr (VI) (Figure 6e) or Fe (II) species (Figure 6f), with no peak shifting of the fluorescence emission maximum observed. The Stern-Volmer relation plots showed good correlation for both Cr (VI) ( $R^2 = 0.9994$ ) and Fe (II) ( $R^2 = 0.9999$ ) giving respective quenching constant values,  $K_{SV} = 0.00624$  (determined from the slope of the line  $y = 0.00624x + 0.01108$ ) for chromate anions (Cr (VI)) and  $K_{SV} = 0.00386$  ( $y = 0.00386x + 0.0383$ ) for ferrous ions (Fe (II)).

The LOD was calculated using the equation  $LOD = 3\sigma/K_{SV}$ , and the LOQ using the equation  $LOQ = 10\sigma/K_{SV}$  ( $\sigma$  is the standard error of the intercept from the Stern-Volmer plots). LOD of 3.62 ppm with LOQ of 11.6 ppm was obtained for Cr (VI) ( $\sigma = 0.00725$ ), and LOD of 1.83 ppm with LOQ of 6.09 ppm for Fe (II) ( $\sigma = 0.00232$ ). The suitability of the CQDs as sensors for both Cr (VI) and Fe (II) was further demonstrated by the stability of the emission intensities for the pure CQDs, [CQDs-Cr (VI)], and [CQDs-Fe (II)] solutions at 446 nm (see Figure S2) showing a negligible variation over time when the samples were subjected to continuous excitation at 360 nm for 1200 seconds.

The aforementioned absence of a noticeable red-shift of the respective emissions related to Cr (VI) and Fe (II) detection (contrary to the observed response of the CQDs to changes in pH, Figure 4c) suggests an alternative mechanism to that involving direct metal ion interactions (Cr (VI) or Fe (II)) with the CQDs surfaces functional groups. The diminishing emissive intensity observed previously for the pH titration profile (Figure 4c) may be attributed to the protonation/deprotonation of the carboxylate groups and/or other moieties resulting in disruption of the surface charge and associated emissivity for the CQDs. Protonation of the various oxygen moieties within the CQDs tight surface entanglement could readily occur due to ease of access of the significantly smaller sized charged particles where other larger cations regardless of charge could not. Deprotonation on the other hand could be considered a consequence of the greater ionization potential of the hydroxide ion across solute-solvent interactions at high concentrations over that of other anions tested.<sup>54</sup> The selectivity of the nano-sensors for Cr (VI) and Fe (II) may then best be attributed to a physical phenomenon called the Inner Filter Effect (IFE).

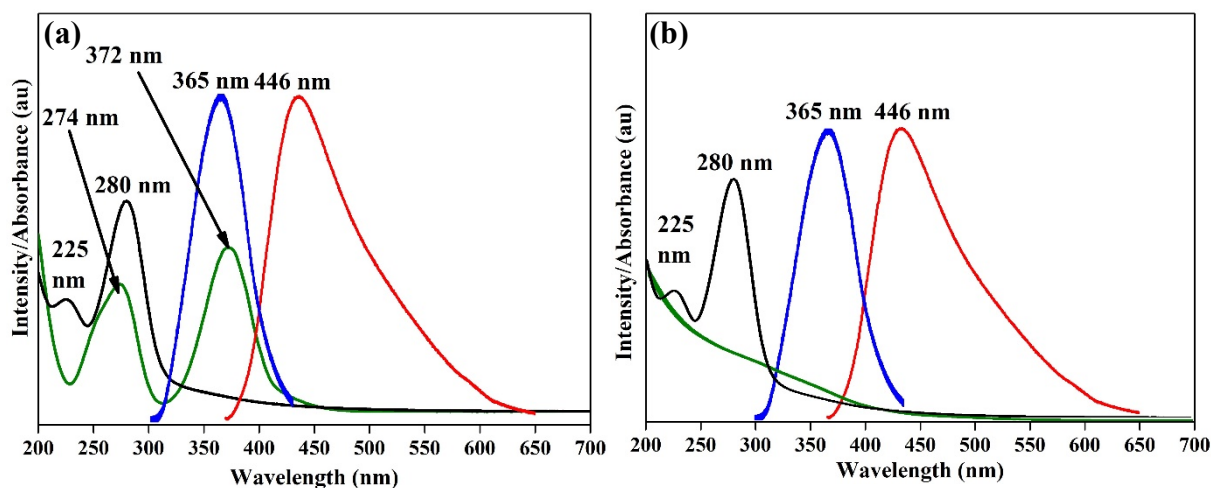


**Figure 7:** Spectral overlap of the normalized UV-Vis absorption bands for the analyte ions (green) and the CHFS-synthesised CQDs (black line), and the excitation spectrum ( $\lambda_{\text{em}} = 446$  nm) (blue line) and emission spectrum ( $\lambda_{\text{ext}} = 365$  nm) (red line) of the CQDs, demonstrating the Inner Filter Effect of (a) Chromate ( $\text{CrO}_4^{2-}$ ) and (b) Ferrous ( $\text{Fe}^{2+}$ ) ions.

The Inner Filter Effect (IFE) is the spectral overlap of the analytes absorption bands ( $\text{CrO}_4^{2-}$  or  $\text{Fe}^{2+}$  ions in these instances) with either or both the excitation and emission band of the substrate (CQDs) as in Figure 7 a-b. An overlap of an excitation band of the CQDs with the analytes absorption band would create an absorptive competition that results in lower excitation of the CQDs, thus emitting far fewer photons with a proportionate decrease in the emission band intensity to the analyte concentration. In this regard, the CQDs excitation and emission bands ( $\lambda_{\text{ext}} = 365$  nm and  $\lambda_{\text{em}} = 446$  nm), have significant overlap with the chromate ( $\text{CrO}_4^{2-}$ ) anions absorption bands centred at 372 nm. There is also a second absorption band of  $\text{CrO}_4^{2-}$  at 274 nm that overlaps with the CQDs most intense absorption band at 280 nm. For Fe (II), a broader band of absorption readily overlaps both the excitation and absorption spectra of CQDs (but to a lesser extent the emission band). Essentially the metal ions have a well-defined electronic structure, smaller size, and higher concentrations in the solution compared to that of the CQDs, thus demonstrate a greater efficiency in not only absorbing any radiation at 360 nm required by the CQDs to produce an excited state emission but also, in the case of  $\text{CrO}_4^{2-}$ , absorb any emitted photons from the CQDs. These processes consequently result in a diminishment of the CQDs fluorescence intensity by either Cr (VI) or Fe (II) ions. The IFE mechanism has been previously explored and applied to nano-sensors for chromium (VI) and iron (II) detection.<sup>19,55,56</sup>

Despite excitation dependence, and a broad FWHM ( $\sim 113$  nm, where 100 nm is characteristic for CQDs), the water soluble CQDs optimal fluorescence emission (446 nm) is

remote from the range for UV excitation (320–380 nm) thus avoiding auto-luminescence, and exhibit stable emission intensities over a wide pH range. In the absence of any doping or surface passivation, its LOD and LOQ for chromium (VI) and iron (II) detection are within range to effectively demonstrate its suitability as a nanosensor, although with lower sensitivity for detection of Cr (VI) compared to our previously reported N-doped CQDS (LOD of 0.365 ppm and LOQ of 1.218 ppm).<sup>27</sup> However, this offers an avenue of exploration and further insight from future studies of CHFS processed CQDs from dopants with glucose.

### Life-Cycle Assessment (LCA)

In pursuit of principles of green chemistry and engineering (IMPROVEMENTS PRODUCTIVELY) and sustainability,<sup>57–61</sup> a streamlined LCA was carried out following ISO14040 and ISO14044 standards and using SimaPro (version 9.1) software with inventory data sourced from the Ecoinvent (version 3.6) database.<sup>62</sup> Two processes involving a batch hydrothermal reactor<sup>63</sup> and the current CHFS synthesis were compared. Two selected LCA indicators were: the global warming potential (GWP) which can be expressed as mass of CO<sub>2</sub>-equivalent (Figure 8a) and the cumulative energy demand (CED) expressed as MJ (see Figure 8b). The GWP values were calculated using the IPCC 2013 method. The CED values were obtained using the ReCiPe midpoint 2016 method.<sup>64</sup> Table S1 from the Supporting Information includes experimental and inventory data (for glucose, water and electricity consumption values), the results of which are shown in Figure 8.

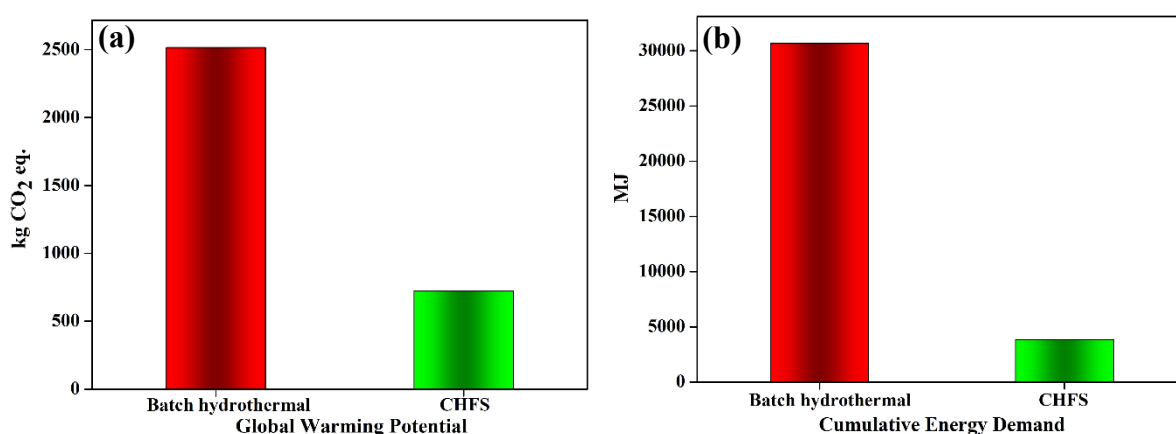


**Figure 8.** (a) Global warming potential (GWP), and (b) cumulative energy demand (CED) indicators for CHFS, and batch synthesis for a normalized yield.

The streamlined LCA results reveal that the CHFS experiment has significantly lower GWP and CED indicators than the comparable batch experiment from the literature<sup>62</sup> (see Figure

8), indicating a very much reduced impact on both climate change and depletion of energy resources. The electricity consumption in both processes makes up the largest contribution to the GWP and CED indicators. When normalising these results with respect to the (lower) synthesis yield obtained for the batch process (0.72 g/6 hr), the GWP and CED indicators are ~ 3.5 and ~8 fold lower respectively (Figure 8), favouring the CHFS process over the batch synthesis process. It is worth noting that, compared to batch synthesis of the CQDs, the CHFS process reaches approximately ~4-fold greater yield (0.46 g/hr) delivering in a continuous mode (real time) *ca.* 7.7 mg min<sup>-1</sup>.

## CONCLUSIONS

The life-cycle assessment confirms that the continuous hydrothermal flow synthesis process is significantly a more efficient and greener route when compared with a conventional batch hydrothermal method for the synthesis of carbon quantum dots. The CDQs were produced utilising a biomass precursor (glucose) as the carbon source and delivered continuously with a yield ~4-fold greater than the conventional process. With excellent uniformity in particle size ( $2.3 \pm 0.5$  nm), pH stability (pH 3 to 10), the water-soluble CQDs exhibit excitation dependent behaviour with an optimum emission peak at 446 nm on excitation at 360 nm. Additionally, the CHFS-produced CQDs exhibited good selectivity and sensitivity for both chromate anions (Cr (VI)) and ferrous ions (Fe (II)), indicating suitability for environmental and biological sensing applications. There is opportunity to further explore and optimise the CQDs potential by introducing various dopants for example, as well as utilising their optical properties in applications in photovoltaics, energy storage and beyond.

## CONFLICT OF INTEREST

The authors have no conflicts of interest to declare.

## ACKNOWLEDGEMENTS

SK and IAB would like to acknowledge the financial support provided by LSBU. The authors would like to acknowledge the technical assistance of Dr Igor Kraev of the Open University Electron Microscopy Suite for HRTEM as well as their corresponding institutes.

**SUPPORTING INFORMATION:** Plot of quantum yield determination *via* integrated fluorescence intensity vs absorbance; Stability analysis of the CQDs in presence of Cr (VI) and Fe (II); PL spectra of carbon quantum dots synthesised in CHFS using glucose and citric acid as carbon precursors; LCA experimental and inventory data.

## REFERENCES

- (1) Wang, Y.; Hu, A. Carbon Quantum Dots: Synthesis, Properties and Applications. *J. Mater. Chem. C* **2014**, *2* (34), 6921–6939. <https://doi.org/10.1039/c4tc00988f>.
- (2) Lim, S. Y.; Shen, W.; Gao, Z. Carbon Quantum Dots and Their Applications. *Chem. Soc. Rev.* **2015**, *44* (1), 362–381. <https://doi.org/10.1039/c4cs00269e>.
- (3) Xu, X.; Ray, R.; Gu, Y.; Ploehn, H. J.; Gearheart, L.; Raker, K.; Scrivens, W. A. Electrophoretic Analysis and Purification of Fluorescent Single-Walled Carbon Nanotube Fragments. *J. Am. Chem. Soc.* **2004**, *126* (40), 12736–12737. <https://doi.org/10.1021/ja040082h>.
- (4) Luo, H.; Papaioannou, N.; Salvadori, E.; Roessler, M. M.; Ploenes, G.; Eck, E. R. H.; Tanase, L. C.; Feng, J.; Sun, Y.; Yang, Y.; Danaie, M.; Belen Jorge, A.; Sapelkin, A.; Durrant, J.; Dimitrov, S. D.; Titirici, M. Manipulating the Optical Properties of Carbon Dots by Fine-Tuning Their Structural Features. *ChemSusChem* **2019**, *12* (19), 4335–4335. <https://doi.org/10.1002/cssc.201902519>.
- (5) Marinovic, A.; Kiat, L. S.; Dunn, S.; Titirici, M.-M.; Briscoe, J. Carbon-Nanodot Solar Cells from Renewable Precursors. *ChemSusChem* **2017**, *10* (5), 1004–1013. <https://doi.org/10.1002/cssc.201601741>.
- (6) Papaioannou, N.; Marinovic, A.; Yoshizawa, N.; Goode, A. E.; Fay, M.; Khlobystov, A.; Titirici, M. M.; Sapelkin, A. Structure and Solvents Effects on the Optical Properties of Sugar-Derived Carbon Nanodots. *Sci. Rep.* **2018**, *8* (1), 1–10. <https://doi.org/10.1038/s41598-018-25012-8>.
- (7) Li, Y.; Zhong, X.; Rider, A. E.; Furman, S. A.; Ostrikov, K. Fast, Energy-Efficient Synthesis of Luminescent Carbon Quantum Dots. *Green Chem.* **2014**, *16* (5), 2566–2570. <https://doi.org/10.1039/c3gc42562b>.
- (8) Ehrat, F.; Bhattacharyya, S.; Schneider, J.; Löf, A.; Wyrwich, R.; Rogach, A. L.; Stolarczyk, J. K.; Urban, A. S.; Feldmann, J. Tracking the Source of Carbon Dot Photoluminescence: Aromatic Domains versus Molecular Fluorophores. *Nano Lett.* **2017**,

- 17 (12), 7710–7716. <https://doi.org/10.1021/acs.nanolett.7b03863>.
- (9) Briscoe, J.; Marinovic, A.; Sevilla, M.; Dunn, S.; Titirici, M. Biomass-Derived Carbon Quantum Dot Sensitizers for Solid-State Nanostructured Solar Cells. *Angew. Chemie - Int. Ed.* **2015**, *54* (15), 4463–4468. <https://doi.org/10.1002/anie.201409290>.
- (10) Wu, P.; Li, W.; Wu, Q.; Liu, Y.; Liu, S. Hydrothermal Synthesis of Nitrogen-Doped Carbon Quantum Dots from Microcrystalline Cellulose for the Detection of Fe<sup>3+</sup> Ions in an Acidic Environment. *RSC Adv.* **2017**, *7* (70), 44144–44153. <https://doi.org/10.1039/c7ra08400e>.
- (11) Chen, W.; Hu, C.; Yang, Y.; Cui, J.; Liu, Y. Rapid Synthesis of Carbon Dots by Hydrothermal Treatment of Lignin. *Materials (Basel)*. **2016**, *9* (3), 184. <https://doi.org/10.3390/ma9030184>.
- (12) Qu, D.; Zheng, M.; Zhang, L.; Zhao, H.; Xie, Z.; Jing, X.; Haddad, R. E.; Fan, H.; Sun, Z. Formation Mechanism and Optimization of Highly Luminescent N-Doped Graphene Quantum Dots. *Sci. Rep.* **2014**, *4*, 1–11. <https://doi.org/10.1038/srep05294>.
- (13) Wang, L.; Sofer, Z.; Pumera, M. Will Any Crap We Put into Graphene Increase Its Electrocatalytic Effect? *ACS Nano* **2020**, *14* (1), 21–25. <https://doi.org/10.1021/acsnano.9b00184>.
- (14) Meng, Y.; Zhang, Y.; Sun, W.; Wang, M.; He, B.; Chen, H.; Tang, Q. Biomass Converted Carbon Quantum Dots for All-Weather Solar Cells. *Electrochim. Acta* **2017**, *257*, 259–266. <https://doi.org/10.1016/j.electacta.2017.10.086>.
- (15) Roy, P.; Chen, P. C.; Periasamy, A. P.; Chen, Y. N.; Chang, H. T. Photoluminescent Carbon Nanodots: Synthesis, Physicochemical Properties and Analytical Applications. *Mater. Today* **2015**, *18* (8), 447–458. <https://doi.org/10.1016/j.mattod.2015.04.005>.
- (16) Luo, X.; Al-Antaki, A. H. M.; Vimalanathan, K.; Moffatt, J.; Zheng, K.; Zou, Y.; Zou, J.; Duan, X.; Lamb, R. N.; Wang, S.; Li, Q.; Zhang, W.; Raston, C. L. Laser Irradiated Vortex Fluidic Mediated Synthesis of Luminescent Carbon Nanodots under Continuous Flow. *React. Chem. Eng.* **2018**, *3* (2), 164–170. <https://doi.org/10.1039/c7re00197e>.
- (17) Liu, M.; Xu, Y.; Niu, F.; Gooding, J. J.; Liu, J. Carbon Quantum Dots Directly Generated from Electrochemical Oxidation of Graphite Electrodes in Alkaline Alcohols and the Applications for Specific Ferric Ion Detection and Cell Imaging. *Analyst* **2016**, *141* (9), 2657–2664. <https://doi.org/10.1039/c5an02231b>.
- (18) Wang, C. C.; Lu, S. Y. Carbon Black-Derived Graphene Quantum Dots Compositing with Carbon Aerogel as a Highly Efficient and Stable Reduction Catalyst for the Iodide/Tri-Iodide Couple. *Nanoscale* **2015**, *7* (3), 1209–1215. <https://doi.org/10.1039/c4nr06118g>.

- (19) Guo, Y.; Chen, Y.; Cao, F.; Wang, L.; Wang, Z.; Leng, Y. Hydrothermal Synthesis of Nitrogen and Boron Doped Carbon Quantum Dots with Yellow-Green Emission for Sensing Cr(VI), Anti-Counterfeiting and Cell Imaging. *RSC Adv.* **2017**, *7* (76), 48386–48393. <https://doi.org/10.1039/c7ra09785a>.
- (20) Goodall, J. B. M.; Kellici, S.; Illsley, D.; Lines, R.; Knowles, J. C.; Darr, J. a. Optical and Photocatalytic Behaviours of Nanoparticles in the Ti-Zn-O Binary System. *RSC Adv.* **2014**, *4*, 31799–31809. <https://doi.org/10.1039/c3ra48030e>.
- (21) Kellici, S.; Acord, J.; Vaughn, A.; Power, N. P.; Morgan, D. J.; Heil, T.; Facq, S. P.; Lampronti, G. I. Calixarene Assisted Rapid Synthesis of Silver-Graphene Nanocomposites with Enhanced Antibacterial Activity. *ACS Appl. Mater. Interfaces* **2016**, *8* (29), 19038–19046. <https://doi.org/10.1021/acsami.6b06052>.
- (22) Kellici, S.; Acord, J.; Ball, J.; Reehal, H. S.; Morgan, D.; Saha, B. A Single Rapid Route for the Synthesis of Reduced Graphene Oxide with Antibacterial Activities. *RSC Adv.* **2014**, *4* (29), 14858–14861. <https://doi.org/10.1039/c3ra47573e>.
- (23) Kellici, S.; Acord, J.; Moore, K. E.; Power, N. P.; Middelkoop, V.; Morgan, D. J.; Heil, T.; Coppo, P.; Baragau, I. A.; Raston, C. L. Continuous Hydrothermal Flow Synthesis of Graphene Quantum Dots. *React. Chem. Eng.* **2018**, *3* (6), 949–958. <https://doi.org/10.1039/c8re00158h>.
- (24) Kellici, S.; Acord, J.; Power, N. P.; Morgan, D. J.; Coppo, P.; Heil, T.; Saha, B. Rapid Synthesis of Graphene Quantum Dots Using a Continuous Hydrothermal Flow Synthesis Approach. *RSC Adv.* **2017**, *7* (24), 14716–14720. <https://doi.org/10.1039/C7RA00127D>.
- (25) Alli, U.; Hettiarachchi, S. J.; Kellici, S. Chemical Functionalisation of 2D Materials by Batch and Continuous Hydrothermal Flow Synthesis. *Chem. - A Eur. J.* **2020**, *26*, 6447–6460. <https://doi.org/10.1002/chem.202000383>.
- (26) Middelkoop, V.; Slater, T.; Florea, M.; Neațu, F.; Danaci, S.; Onyenkeadi, V.; Boonen, K.; Saha, B.; Baragau, I.-A.; Kellici, S. Next Frontiers in Cleaner Synthesis: 3D Printed Graphene-Supported CeZrLa Mixed-Oxide Nanocatalyst for CO<sub>2</sub> Utilisation and Direct Propylene Carbonate Production. *J. Clean. Prod.* **2019**, *214*, 606–614. <https://doi.org/10.1016/j.jclepro.2018.12.274>.
- (27) Baragau, I.-A.; Power, N. P.; Morgan, D. J.; Heil, T.; Lobo, A.; Roberts, S.; Titirici, M.; Kellici, S. Continuous Hydrothermal Flow Synthesis of Blue- Luminescent, Excitation-Independent Nitrogen- Doped Carbon Quantum Dots as Nanosensors. *J. Mater. Chem. A* **2020**, *8* (6), 3270–3279. <https://doi.org/10.1039/c9ta11781d>.
- (28) Zhang, Y.-L.; Wang, L.; Zhang, H.-C.; Liu, Y.; Wang, H.-Y.; Kang, Z.-H.; Lee, S.-T.

- Graphitic Carbon Quantum Dots as a Fluorescent Sensing Platform for Highly Efficient Detection of  $\text{Fe}^{3+}$  Ions. *RSC Adv.* **2013**, 3 (11), 3733–3738. <https://doi.org/10.1039/c3ra23410j>.
- (29) Xie, Z.; Sun, X.; Jiao, J.; Xin, X. Ionic Liquid-Functionalized Carbon Quantum Dots as Fluorescent Probes for Sensitive and Selective Detection of Iron Ion and Ascorbic Acid. *Colloids Surfaces A Physicochem. Eng. Asp.* **2017**, 529 (April), 38–44. <https://doi.org/10.1016/j.colsurfa.2017.05.069>.
- (30) Dong, Y.; Wang, R.; Li, G.; Chen, C.; Chi, Y.; Chen, G. Polyamine-Functionalized Carbon Quantum Dots as Fluorescent Probes for Selective and Sensitive Detection of Copper Ions. *Anal. Chem.* **2012**, 84 (14), 6220–6224. <https://doi.org/10.1021/ac3012126>.
- (31) Guo, Y.; Wang, Z.; Shao, H.; Jiang, X. Hydrothermal Synthesis of Highly Fluorescent Carbon Nanoparticles from Sodium Citrate and Their Use for the Detection of Mercury Ions. *Carbon N. Y.* **2013**, 52, 583–589. <https://doi.org/10.1016/j.carbon.2012.10.028>.
- (32) Shen, P.; Xia, Y. Synthesis-Modification Integration: One-Step Fabrication of Boronic Acid Functionalized Carbon Dots for Fluorescent Blood Sugar Sensing. *Anal. Chem.* **2014**, 86 (11), 5323–5329. <https://doi.org/10.1021/ac5001338>.
- (33) Wang, Q.; Huang, X.; Long, Y.; Wang, X.; Zhang, H.; Zhu, R.; Liang, L.; Teng, P.; Zheng, H. Hollow Luminescent Carbon Dots for Drug Delivery. *Carbon N. Y.* **2013**, 59, 192–199. <https://doi.org/10.1016/j.carbon.2013.03.009>.
- (34) Kalaiyarasan, G.; Hemlata, C.; Joseph, J. Fluorescence Turn-On, Specific Detection of Cystine in Human Blood Plasma and Urine Samples by Nitrogen-Doped Carbon Quantum Dots. *ACS Omega* **2019**, 4 (1), 1007–1014. <https://doi.org/10.1021/acsomega.8b03187>.
- (35) Song, Z.; Quan, F.; Xu, Y.; Liu, M.; Cui, L.; Liu, J. Multifunctional N,S Co-Doped Carbon Quantum Dots with PH- and Thermo-Dependent Switchable Fluorescent Properties and Highly Selective Detection of Glutathione. *Carbon N. Y.* **2016**, 104, 169–178. <https://doi.org/10.1016/j.carbon.2016.04.003>.
- (36) Titirici, M.-M.; White, R. J.; Brun, N.; Budarin, V. L.; Su, D. S.; del Monte, F.; Clark, J. H.; MacLachlan, M. J. Sustainable Carbon Materials. *Chem. Soc. Rev.* **2015**, 44 (1), 250–290. <https://doi.org/10.1039/C4CS00232F>.
- (37) Titirici, M. M. Hydrothermal Carbons: Synthesis, Characterization, and Applications. In *Novel Carbon Adsorbents*; 2012; pp 351–399. <https://doi.org/10.1016/B978-0-08-097744-7.00012-0>.
- (38) Yang, S.; Sun, J.; Li, X.; Zhou, W.; Wang, Z.; He, P.; Ding, G.; Xie, X.; Kang, Z.; Jiang, M. Large-Scale Fabrication of Heavy Doped Carbon Quantum Dots with Tunable-

- Photoluminescence and Sensitive Fluorescence Detection. *J. Mater. Chem. A* **2014**, *2* (23), 8660–8667. <https://doi.org/10.1039/c4ta00860j>.
- (39) Wu, F.; Su, H.; Wang, K.; Wong, W. K.; Zhu, X. Facile Synthesis of N-Rich Carbon Quantum Dots from Porphyrins as Efficient Probes for Bioimaging and Biosensing in Living Cells. *Int. J. Nanomedicine* **2017**, *12*, 7375–7391. <https://doi.org/10.2147/IJN.S147165>.
- (40) Hirayama, T. Fluorescent Probes for the Detection of Catalytic Fe(II) Ion. *Free Radic. Biol. Med.* **2019**, *133*, 38–45. <https://doi.org/10.1016/j.freeradbiomed.2018.07.004>.
- (41) Liu, Y.; Hu, J.; Li, Y.; Wei, H. P.; Li, X. S.; Zhang, X. H.; Chen, S. M.; Chen, X. Q. Synthesis of Polyethyleneimine Capped Carbon Dots for Preconcentration and Slurry Sampling Analysis of Trace Chromium in Environmental Water Samples. *Talanta* **2015**, *134*, 16–23. <https://doi.org/10.1016/j.talanta.2014.11.001>.
- (42) Yuan, F.; Yuan, T.; Sui, L.; Wang, Z.; Xi, Z.; Li, Y.; Li, X.; Fan, L.; Tan, Z.; Chen, A.; Jin, M.; Yang, S. Engineering Triangular Carbon Quantum Dots with Unprecedented Narrow Bandwidth Emission for Multicolored LEDs. *Nat. Commun.* **2018**, *9* (2249), 1–11. <https://doi.org/10.1038/s41467-018-04635-5>.
- (43) da Silva Souza, D. R.; Caminhas, L. D.; de Mesquita, J. P.; Pereira, F. V. Luminescent Carbon Dots Obtained from Cellulose. *Mater. Chem. Phys.* **2018**, *203*, 148–155. <https://doi.org/10.1016/j.matchemphys.2017.10.001>.
- (44) G. Beamson and D. Briggs. *High Resolution XPS of Organic Polymers: The Scienta ESCA300 Database*; WILEY-Interscience, 1992. <https://doi.org/https://doi.org/10.1021/ed070pA25.5>.
- (45) Javed, M.; Saqib, A. N. S.; Ata-ur-Rehman; Ali, B.; Faizan, M.; Anang, D. A.; Iqbal, Z.; Abbas, S. M. Carbon Quantum Dots from Glucose Oxidation as a Highly Competent Anode Material for Lithium and Sodium-Ion Batteries. *Electrochim. Acta* **2019**, *297*, 250–257. <https://doi.org/10.1016/j.electacta.2018.11.167>.
- (46) López-Díaz, D.; López Holgado, M.; García-Fierro, J. L.; Velázquez, M. M. Evolution of the Raman Spectrum with the Chemical Composition of Graphene Oxide. *J. Phys. Chem. C* **2017**, *121* (37), 20489–20497. <https://doi.org/10.1021/acs.jpcc.7b06236>.
- (47) Moon, I. K.; Lee, J.; Ruoff, R. S.; Lee, H. Reduced Graphene Oxide by Chemical Graphitization. *Nat. Commun.* **2010**, *1* (73), 1–6. <https://doi.org/10.1038/ncomms1067>.
- (48) Ding, H.; Yu, S. B.; Wei, J. S.; Xiong, H. M. Full-Color Light-Emitting Carbon Dots with a Surface-State-Controlled Luminescence Mechanism. *ACS Nano* **2016**, *10* (1), 484–491. <https://doi.org/10.1021/acs.nano.5b05406>.

- (49) Yang, Z. C.; Wang, M.; Yong, A. M.; Wong, S. Y.; Zhang, X. H.; Tan, H.; Chang, A. Y.; Li, X.; Wang, J. Intrinsically Fluorescent Carbon Dots with Tunable Emission Derived from Hydrothermal Treatment of Glucose in the Presence of Monopotassium Phosphate. *Chem. Commun.* **2011**, *47* (42), 11615–11617. <https://doi.org/10.1039/c1cc14860e>.
- (50) Zhitkovich, A. Chromium in Drinking Water: Sources, Metabolism, and Cancer Risks. *Chem. Res. Toxicol.* **2011**, *24* (10), 1617–1629. <https://doi.org/10.1021/tx200251t>.
- (51) Costa, M.; Klein, C. B. Toxicity and Carcinogenicity of Chromium Compounds in Humans. *Crit. Rev. Toxicol.* **2006**, *36* (2), 155–163. <https://doi.org/10.1080/10408440500534032>.
- (52) Pellerin, C.; Booker, S. M. Reflections on Hexavalent Chromium: Health Hazards of an Industrial Heavyweight. *Environ. Health Perspect.* **2000**, *108* (9), 402–407. <https://doi.org/10.1289/ehp.108-a402>.
- (53) Neilands, J. B. A Brief History of Iron Metabolism. *Biol. Met.* **1991**, *4*, 1–6. <https://doi.org/https://doi.org/10.1007/BF01135550>.
- (54) Opalka, D.; Pham, T. A.; Sprik, M.; Galli, G. The Ionization Potential of Aqueous Hydroxide Computed Using Many-Body Perturbation Theory. *J. Chem. Phys.* **2014**, *141* (3). <https://doi.org/10.1063/1.4887259>.
- (55) Zheng, M.; Xie, Z.; Qu, D.; Li, D.; Du, P.; Jing, X.; Sun, Z. On-off-on Fluorescent Carbon Dot Nanosensor for Recognition of Chromium(VI) and Ascorbic Acid Based on the Inner Filter Effect. *ACS Appl. Mater. Interfaces* **2013**, *5* (24), 13242–13247. <https://doi.org/10.1021/am4042355>.
- (56) Sun, W.; Du, Y.; Wang, Y. Study on Fluorescence Properties of Carbogenic Nanoparticles and Their Application for the Determination of Ferrous Succinate. *J. Lumin.* **2010**, *130* (8), 1463–1469. <https://doi.org/10.1016/j.jlumin.2010.03.013>.
- (57) Tang, S. Y.; Bourne, R. A.; Smith, R. L.; Poliakoff, M. The 24 Principles of Green Engineering and Green Chemistry: “IMPROVEMENTS PRODUCTIVELY.” *Green Chem.* **2008**, *10* (3), 268. <https://doi.org/10.1039/b719469m>.
- (58) Stieberova, B.; Zilka, M.; Ticha, M.; Freiberg, F.; Caramazana-González, P.; McKechnie, J.; Lester, E. Sustainability Assessment of Continuous-Flow Hydrothermal Synthesis of Nanomaterials in the Context of Other Production Technologies. *J. Clean. Prod.* **2019**, *241*. <https://doi.org/10.1016/j.jclepro.2019.118325>.
- (59) Tsang, M. P.; Philippot, G.; Aymonier, C.; Sonnemann, G. Supercritical Fluid Flow Synthesis to Support Sustainable Production of Engineered Nanomaterials: Case Study of Titanium Dioxide. *ACS Sustain. Chem. Eng.* **2018**, *6* (4), 5142–5151.

<https://doi.org/10.1021/acssuschemeng.7b04800>.

- (60) Patel, D.; Kellici, S.; Saha, B. Green Process Engineering as the Key to Future Processes. *Processes* **2014**, *2* (1), 311–332. <https://doi.org/10.3390/pr2010311>.
- (61) Baragau, I.; Lu, Z.; Power, P.N.; Morgan, J.D.; Bowen, J.; Diaz, P.; Kellici, S. Continuous Hydrothermal Flow Synthesis of S-Functionalised Carbon Quantum Dots for Enhanced Oil Recovery. *Chem. Eng. J.* **2021**, *405*, 127563. <https://doi.org/10.1016/j.cej.2020.126631>
- (62) Wernet, G.; Bauer, C.; Steubing, B.; Reinhard, J.; Moreno-Ruiz, E.; Weidema, B. The Ecoinvent Database Version 3 (Part I): Overview and Methodology. *Int. J. Life Cycle Assess.* **2016**, *21* (9), 1218–1230. <https://doi.org/10.1007/s11367-016-1087-8>.
- (63) Jing, S.; Zhao, Y.; Sun, R. C.; Zhong, L.; Peng, X. Facile and High-Yield Synthesis of Carbon Quantum Dots from Biomass-Derived Carbons at Mild Condition. *ACS Sustain. Chem. Eng.* **2019**, *7* (8), 7833–7843. <https://doi.org/10.1021/acssuschemeng.9b00027>.
- (64) Huijbregts, M. A. J.; Steinmann, Z. J. N.; Elshout, P. M. F.; Stam, G.; Verones, F.; Vieira, M.; Zijp, M.; Hollander, A.; van Zelm, R. ReCiPe2016: A Harmonised Life Cycle Impact Assessment Method at Midpoint and Endpoint Level. *Int. J. Life Cycle Assess.* **2017**, *22* (2), 138–147. <https://doi.org/10.1007/s11367-016-1246-y>.

**For Table of Contents Use Only**

Carbon quantum dots, produced in a continuous mode via a rapid, efficient and green synthetic approach, exhibit optimistic nano-sensing properties.

